



Alexandria University
Alexandria Engineering Journal

www.elsevier.com/locate/aej
www.sciencedirect.com



Experimental Examination for the Electric Power Generation of a Commercial Small-scale Wind Turbine with Modified Aerodynamic Design

Mahmoud E. Hasan^{a,*}, Abdelgalil Eltayesh^a, Mohamed I. Awaad^b,
Hesham M. El-Batsh^{a,c}

^a Mechanical Department, Benha Faculty of Engineering, Benha University, Egypt

^b Electrical Department, Benha Faculty of Engineering, Benha University, Egypt

^c Currently Professor and Dean of Higher Institute of Engineering and Technology at Mahala El-Kobra, Egypt

Received 20 February 2022; revised 28 June 2022; accepted 24 August 2022

KEYWORDS

Small-scale HAWT;
Experimental tests;
CFD simulations;
Wind

Abstract Small-scale horizontal axis wind turbines (SSHAWT) have recently gained more interest due to fuel shortages and environmental issues. Generally, they are installed close to the ground in the wind boundary layer, where the velocity is relatively small. This study aims to evaluate the performance of a commercial SSHAWT and to modify rotor design based on wind velocity in the field. The experimental measurements are performed to examine a commercial 1.5 m radius rotor of 1 kW SSHAWT, which was designed at a rated velocity of about 8 m/s. The CFD calculations are performed as well to understand flow characteristics and to verify the experimental measurements. In the experimental procedure, the test of the wind turbine with a permanent magnet synchronous generator showed that at a wind velocity of 5 and 6 m/s, the highest generated power is 163.9 and 306 W corresponding to power coefficients of 0.255 and 0.28 when AC voltage of the generator is 24.4 and 37.76 V, the DC voltage after rectified 22 and 34 V, and the load current 7.45 and 9 A, respectively. Then the available wind velocity was measured in the field, and the average velocity was 4 m/s. Therefore, a more appropriate rotor is designed based on field velocity. The CFD calculations are used to test the new rotor. The results clarify that for the new rotor, the maximum blade's power coefficient is enhanced by more than 60 % compared to the commercial rotor.

© 2022 THE AUTHORS. Published by Elsevier BV on behalf of Faculty of Engineering, Alexandria University. This is an open access article under the CC BY license (<http://creativecommons.org/licenses/by/4.0/>).

1. Introduction

Wind power generation is the fastest-growing energy technology among different renewable energy sources. Wind turbine systems are classified into two types based on the outward appearance of their blades: horizontal-axis wind turbines

* Corresponding author.

Peer review under responsibility of Faculty of Engineering, Alexandria University.

<https://doi.org/10.1016/j.aej.2022.08.040>

1110-0168 © 2022 THE AUTHORS. Published by Elsevier BV on behalf of Faculty of Engineering, Alexandria University.

This is an open access article under the CC BY license (<http://creativecommons.org/licenses/by/4.0/>).

Nomenclature

A	Amperes	Re	Reynolds number
c	Airfoil chord (m)	r	Blade radius at rotor plane (m)
D	Drag coefficient	V	Free stream velocity of wind (m/s)
C_l	Lift coefficient of an airfoil	V_r	Airfoil relative wind velocity (m/s)
C_d	Drag coefficient of an airfoil	V	Dimensionless wind velocity
C_p	Local power coefficient	α	Angle of attack ($^\circ$)
$C_{p_{max}}$	Maximum power coefficient	ρ	Air density (kg/m^3)
C_{p_m}	Mechanical power coefficient	ω	Angular velocity (S^{-1})
C_{p_e}	Electrical power coefficient	β	Pitch angle ($^\circ$)
L	Drag coefficient	λ	Tip velocity ratio of rotor
R	Radius of wind turbine rotor (m)		

(HAWT) and vertical-axis wind turbines (VAWT). Because HAWT blades always sweep towards the wind, they collect more wind energy than VAWT blades. The HAWT can be widely used in commercial large-scale electric power generation and in addition to small-scale power generation purposes.

In wind farms, the large-scale horizontal axis wind turbines (LSHAWTs) are installed in large numbers due to the availability of the wasted space and are exploited in the link to the electric grid. These LSHAWTs usually operate at relatively high wind velocity, reaching more than 10 m/s [1]. Nevertheless, these velocities are not easy to be achieved in the residential areas due to the surrounding areas and the wind boundary layer. These topographies significantly influence the characteristics of wind in which wind shear is increased by higher densely populated areas, which requires more energy. So, the studies on the LSHAWT with blades in the range from 30 to 40 m long are performed at the high elevation range from 60 to 80 m, and it is achievable in the tower [2]. The design of these devices is operated depending on the data from the site, which is often provided in the wind Atlas and includes wind

velocity beyond the ground's boundary layer at levels of roughly 50 m [3]. As a result, LSHAWTs are unsuited for use in residential regions. So, in residential areas, the attention is focused on domestic small-scale horizontal axis wind turbines (SSHAWTs) than LSHAWTs. These SSHAWTs are commonly available on the market with rotor diameters rang-

Table 1 The main specifications of the Foshan Ouyad factory S-rotor wind turbine.

Parameter	Value	Parameter	Value
Generator model	FD3.0–1000	Blade material (quantity)	Fiberglass (3)
Rated power (W)	1000	Rated wind velocity (m/s)	8
Cut-in wind velocity (m/s)	3	Rated rotating speed (rpm)	350
AC Voltage (V)	48	Current (A)	12

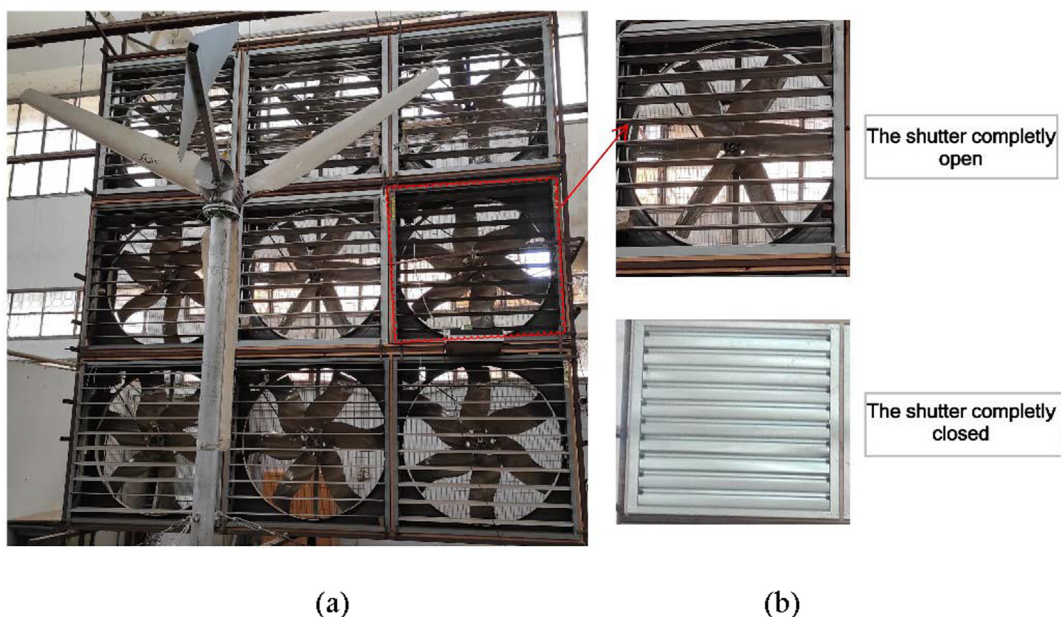


Fig. 1 (a) The open grid fans. (b) The shutter mechanism.

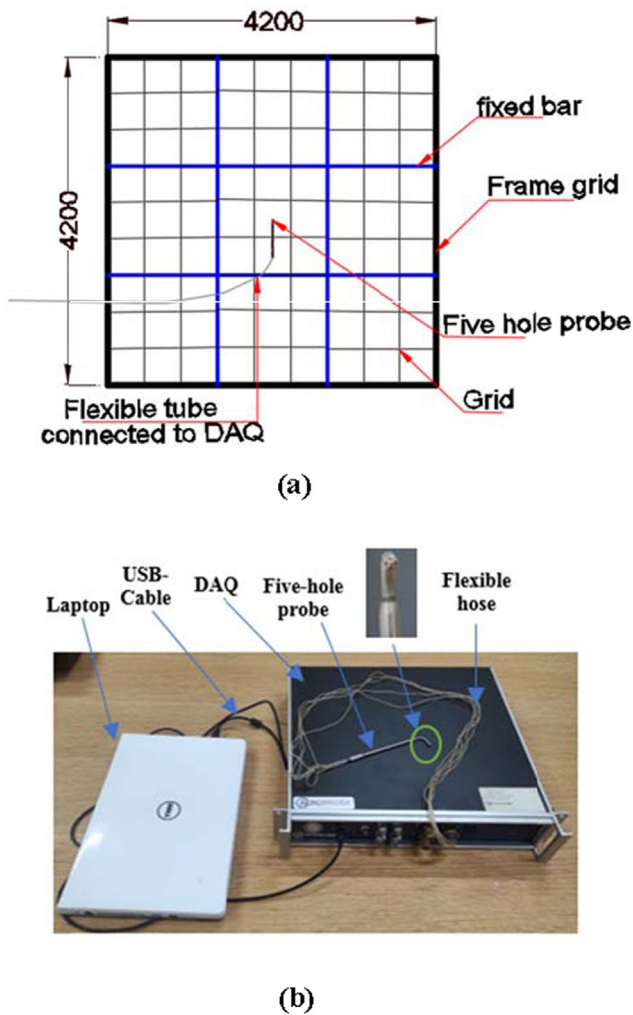


Fig. 2 (a) The grid meshes. (b) The five-hole probe system.

ing from 3 m to 10 m [4]. Also, These SSHAWTs can be utilized to generate electricity in urban areas where the electric grid is unavailable. So, the interest in increasing the generated power from the SSHAWT becomes more significant.

The SSHAWT is permanently installed near the ground, where the wind velocity is variable based on the surrounding area. Also, the rated velocity for the full scale of domestic SSHAWT is still high compared to the velocities that can be captured from the residential and urban areas for all places, as in this work and Pagnini et al. [5]. So, the researchers aim to expand the use of the SSHAWT in the commercial and residential areas by redesigning the SSHAWT with suitable airfoils and increasing its performance.

Giguere and Selig [6] recommended the benefits of using four airfoils on the aerodynamic performance of the SSHAWT with a 1 – 5 kW power range. The airfoils were SG6040 airfoil at the root till 30 % of the blade, and SG6041, SG6042, and SG6043 were distributed along the rest of the blade. By using these airfoils, researchers have attempted to design SSHAWT via various approaches. Gupta et al. [7] performed theoretically the aerodynamic performance for two different rotors of SSHAWT, which has a 2.6 m diameter using Blade element

momentum theory (BEMT). Thereafter, the results were validated using computational fluid dynamics (CFD) calculation. The results obtained by CFD are almost identical to those obtained by the theoretical one, and the SG-rotor had the best performance. Also, Aung et al. [8] investigated numerically the aerodynamic performance of two different wind turbine rotors at Re of 5×10^5 . Also, it was reported that the SG6043 is the best blade in low wind velocity areas. Furthermore, Karthikeyan and Suthakar [9] used XFOIL software to investigate the aerodynamic characteristics of different airfoils at low Re . The result showed that the SG airfoils gave the maximum lift to drag ratio at the small range of angle of attack (α). Also, Nath and Bhattacharjee [10] used BEM and experimental techniques to compare the performance analysis of several types of airfoils using a rotor diameter of 1.2 m at low Re . The study was carried out using four different airfoils, namely; SG6043, SG6042, NACA4415, and NACA4420. It was found that the SG6043 airfoil gives the maximum lift to drag coefficient equal to 176 at α of 2° and Re of 200000. Moreover, Moussa [11] investigates experimentally and numerically the performance of a HAWT at a wind speed ranging between 2 and 6 m/s. Experiments were conducted outdoors, while numerical simulations were performed using computational fluid dynamics with SST k- ω turbulence model. The generated electrical power was computed using the current and voltage measurements, accounting for cable losses and the inverter's efficiency. According to both the experiment and numerical results, a tip speed ratio of 5.39 gives a maximum power coefficient of 0.24. Furthermore, the numerical results demonstrate that the turbulence intensity increases considerably concerning the tip speed ratio as the tip speed ratio increases. Accordingly, the turbine rotor rotation speed affects the pressure discontinuities generated. Moreover, Experiment results demonstrate good agreement with empirical and numerical models of the power coefficient evolution with a maximum error of around 5 %.

Also, the composite airfoils showed the highly effective performance of the SSHAWT at low wind speeds. So, Mwanyika et al. [12] examined the effect of using composite airfoil SSHAWT in low wind speed applications for a standalone system. The BEM theory was utilized to create the five rotor blades, and then the rotor was modeled using SolidWorks software. SG6042 and SG6043 were the composite airfoils used. CFD was also used to evaluate the best rotor design. The results showed that the composite airfoil wind turbine blade had enhanced performance, with wind power output ranging between 4966 and 5258 W and rotor power coefficients ranging between 0.443 and 0.457. The blade with a design angle of attack of 6° performed the best. Furthermore, Chaudhary et al. [13] investigated experimentally 0.5 m rotor diameter of SSHAWT in a low wind speed region. The selected airfoils from the analysis for the study were E216 and NACA2412 airfoils. The Q-Blade was used to analyze the aerodynamics of the airfoils at solidity less than 20 %. The experimental results showed that the mixed rotor yields the maximum performance with a C_p of 0.45 at a tip speed ratio of 6. In general, Wind turbines with mixed airfoils were the best suitable for low wind speed applications.

Also, the material and the start-up of the blade are the essential factors that affect the performance of the wind turbine. So, Sessarego and Wood [14] optimized small wind turbines to improve the turbine start-up, power extraction, and

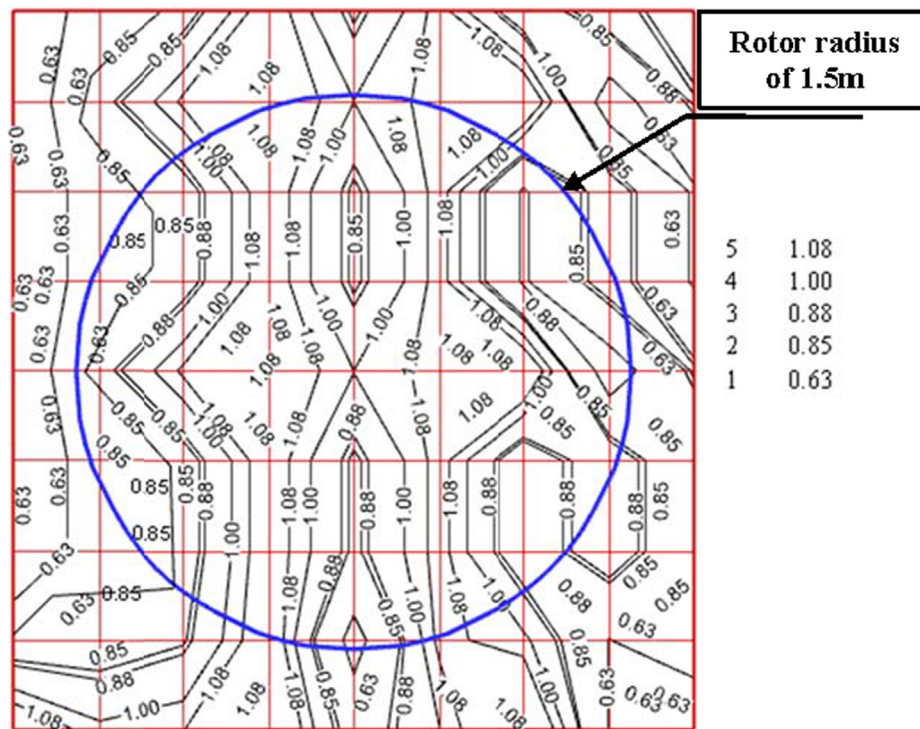


Fig. 3 The contours of the measured dimensionless inlet velocity.

minimize mass. They used SG6043 with 10% thickness and SD7062 with 14% thickness were mixed to make a set of blades with four different materials. They found that the wind turbine's starting time mainly depends on the blade's inertia and the blade material. Also, the SG6043 airfoil is appropriate for the E-glass & polyester resin, the flax & polyester resin, and the timber materials.

For variable-speed turbines, the National Renewable Energy Laboratory (NREL) recommended using mixed S-Series airfoils (S833, S834, and S835) in wind turbines with rotor diameters of 1–3 m. So, M. Hasan et al. [15] investigated the performance of using the (NREL) airfoils type S series on a 5.5 m radius rotor (R) of SSHAWT analytically and numerically. The performance was studied analytically by using BEMT and numerically by using the 3D simulations with SST k-omega turbulence model. The first rotor consists of a single airfoil profile, S833, and the second rotor consists of mixed three airfoils S823, S833, and S822 as the hub, primary, and tip, respectively. It was found that the mixed airfoils gave the best aerodynamic performance. Selig and McGranahan [16] tested the 6 airfoils as follows: E387, FX 63-137, S822, S834, SD2030, and SH3055 in the wind tunnel for small wind turbine application. The aerodynamic performance was studied at various Re such as 100,000, 150,000, 200,000, 350,000 and 500,000. Flow quality oil flow visualization and performance data on the E387 airfoil were studied before the tests began for comparing with the data from the National Aeronautics and Space Administration (NASA). The new results are favorable for comparison with the NASA data. Also, the results showed that; In low Re, the S834 is better than the S822 airfoil. Pamuji and BRAMANTYA [17] investigated the performance and fluid flow characteristics numerically using 2 & 3 blades of

counter-rotating wind turbine (CRWT) for a 3 m diameter rotor using the NREL mixed airfoils such as S835 at the root, S833 at the main and S834 at the tip. The investigation was performed at a wind velocity of 4.5 m/s and λ of 5. The SST k-omega turbulence model was used for the 3D simulations. The results showed that the characteristics of steady angular velocity (ω) of the 2-bladed CRWT were higher than the 3-bladed CRWT. However, by comparing the performance, the 3-bladed CRWT gives a better performance in terms of time to reach their steady angular velocities than the 2-bladed CRWT.

From the previous works, The NREL has several special-purpose airfoil families for SSHAWTs; among those, the NREL's S8-xx series, such as (S833- S834- S835) airfoils and the SG60xx series such as (SG6040- SG6043) airfoils. These series are suitable for small-scale wind turbine blades at low wind velocities. To the author's knowledge, for commercial SSHAWTs, there is no clear data for using these series in this application due to the difficulty of collecting the data of used airfoils of the commercial SSHAWT in the market. This study aims to test experimentally and numerically the performance of the commercial wind turbine available in the market, which is designed from S833, S834, and S835 airfoils that are referred to as S-rotor at the wind turbine laboratory, department of mechanical Engineering, Benha University. The turbine's performance is examined by measuring the electrical power and estimating the mechanical and electrical efficiencies. The study also aims to design numerically and examine the performance of the SG-rotor based on wind velocity in the field with the same diameter as the S-rotor using SG6040 and SG6043 airfoils and referred to as SG-rotor. The SG-rotor was designed based on the average wind velocity measured in the Benha University, Obour Campus.

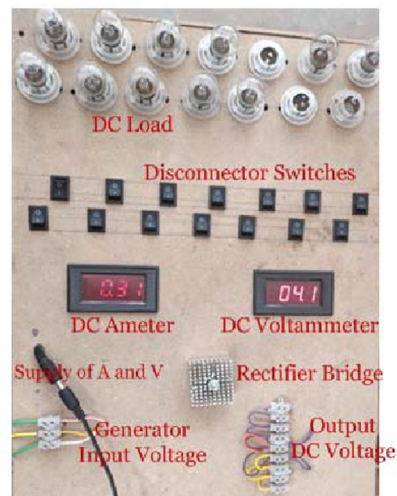
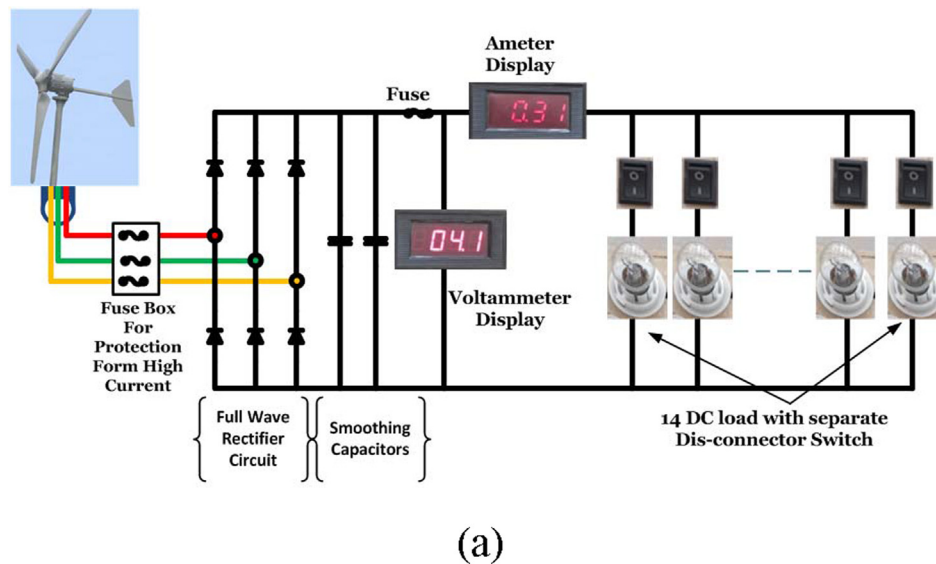


Fig. 4 (a) The schematic diagram for the electrical load system (b) The photo of the electrical control panel.

2. Experimental technique

2.1. Experimental setup

The wind is characterized by unsteady flow patterns. In residential areas, these patterns become non-uniform [18]. Almost all previous studies on the SSHAWTs tested the scale models and used dimensional analysis to represent the full-scale performance, where the similarity is always questionable. In this study, a full-scale commercial 1.5 m radius of SSHAWT was examined in the wind turbine laboratory, Benha Faculty of Engineering, Benha University. The rotor had three blades with the S-rotor profile. The test was carried out using nine centrifugal shutter exhaust fans, model DJF-1380.

These fans were divided into three sections and were connected to steel structures working as open grid fans, as shown in Fig. 1 (a). The overall dimension of the open grid fans is (4200 mm × 4200 mm), and the height of the first section from

the floor is 1000 mm. The important specification of the selected fans was the shutter opening mechanism with a double swung drop hammer, as shown in Fig. 1 (b), which can ensure the shutter is completely opened or closed to reduce the distance required to obtain the fully developed flow.

A control panel was used to control each fan separately, enabling us to simulate the wind field pattern. The rotational speed of each fan was controlled by using the frequency changer model S3100 Multi-Function Vector Control Inverter with a range of 11–15 kW to give variable wind velocities with a range of 0–7 m/s affecting the wind turbine wheel velocity. Also, this inverter can be used to simulate the transient flow by varying the frequency of the fans with time. However, in this study, all fans were allowed to operate at the same velocity. Each fan had a dimension of 1400mm x 1400 mm and air-flow of 44,000 m³/hr. The wind turbine was placed at the center point of the open grid fans and positioned at 2000 mm (1.5 radii of the turbine) from the open fan grid exit.

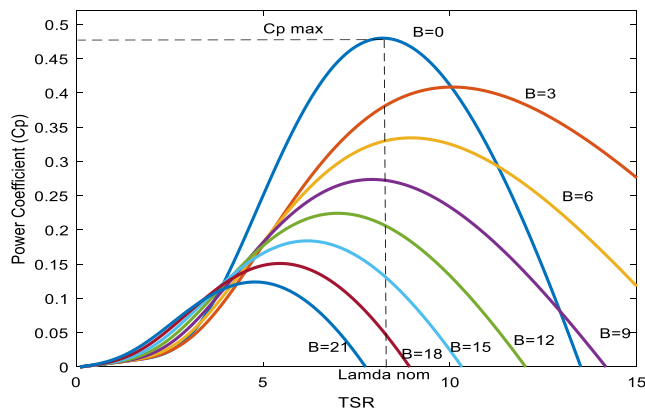


Fig. 5 The impact of different blade pitches on the performance of a small wind turbine [27 28].

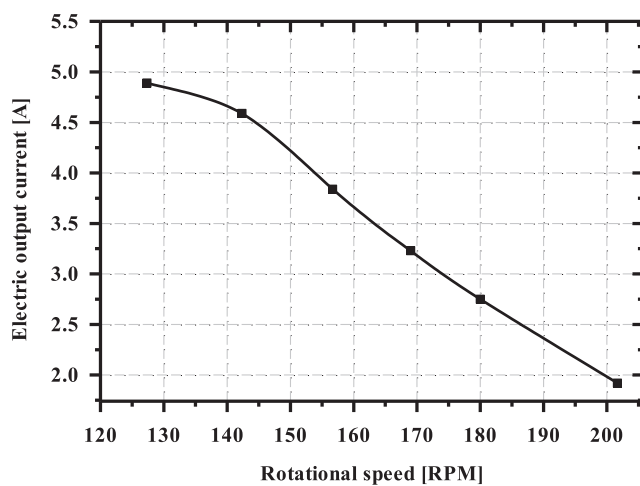
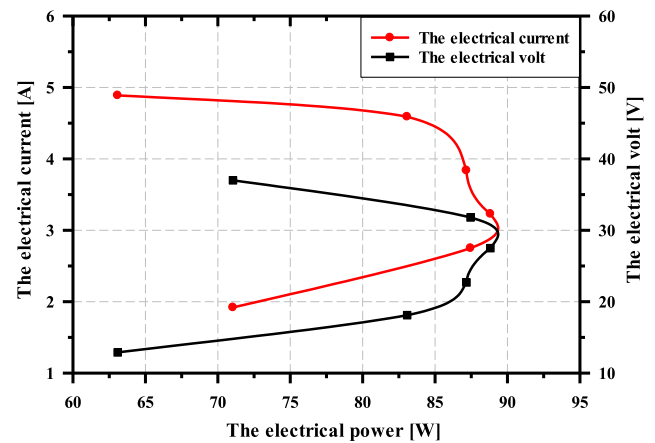


Fig. 6 The relation between the load current and the rotor speed at a wind velocity of 4 m/s.

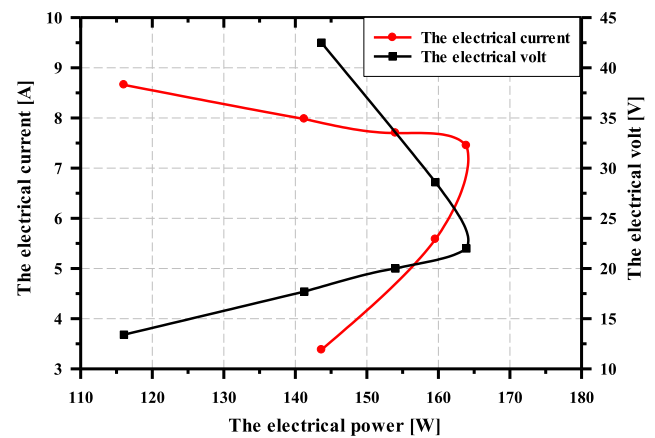
The wind turbine was manufactured by the Foshan Ouyad factory [19], and its specifications are shown in Table 1. The turbine is directly coupled to the 1 kW permanent magnet synchronism generator (PMSG).

Due to the relatively small distance between the fans and the wind turbine, measuring the velocity variation along the fans was required. So, a five-hole probe (AP4K USB system type) with maximum flow velocity up to 30 m/s and accuracy $\pm 0.8\%$ of velocity magnitude was positioned on a grid mesh of 81 cells, as shown in Fig. 2 (a). This probe was connected to the Data acquisition (DAQ) system (ATX sensor module) manufactured by Aeroprobe International Company in the USA. More details on the measurement procedure could be found in [20]. The sampling rate of this DAQ reached up to 10,000 sample/s. The velocity magnitude was obtained from Aeroacquire software via the laptop, as shown in Fig. 2 (b).

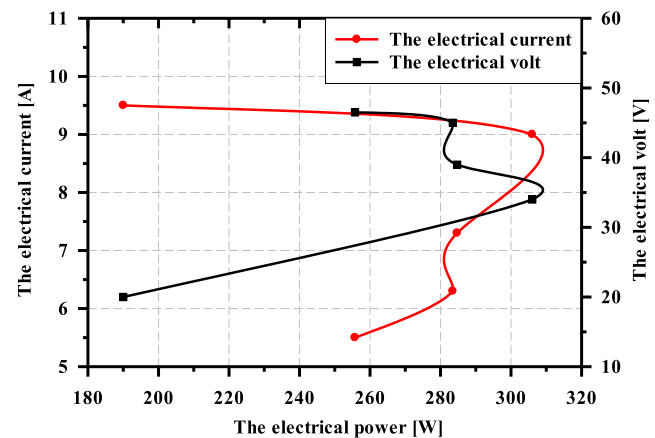
Fig. 3 showed the contour of the measured dimensionless inlet velocity (\tilde{V}) along with the open grid fans. The average inlet velocity (\bar{V}) was calculated using the energy-weighted



(a)



(b)



(c)

Fig. 7 Measured Electrical Power, Voltage, and Current for wind velocities (a) 4 m/s (b) 5 m/s (c) 6 m/s.

average of the measured velocities for all cells by changing the load. The velocity variation was about $\pm 10\%$ of the average velocity, which is acceptable considering wind velocity variation as introduced by [21]. It also agrees with open jet flow measurement from a wind turbine as obtained by Abdelsalam et al. [22].

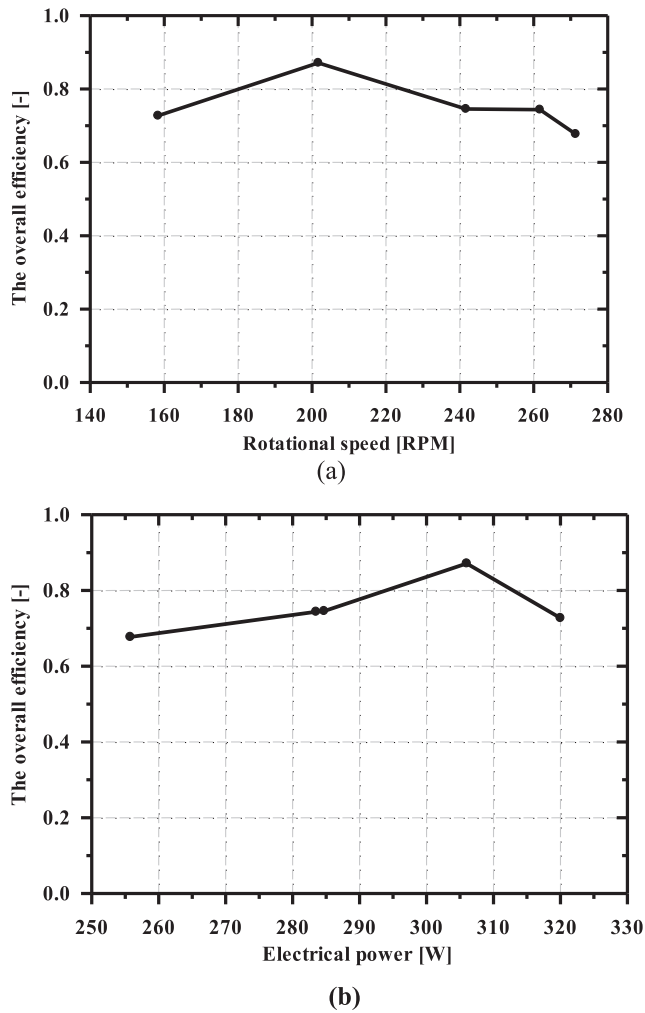


Fig. 8 The overall efficiency relations with (a) The rotational speed and (b) The electrical power.

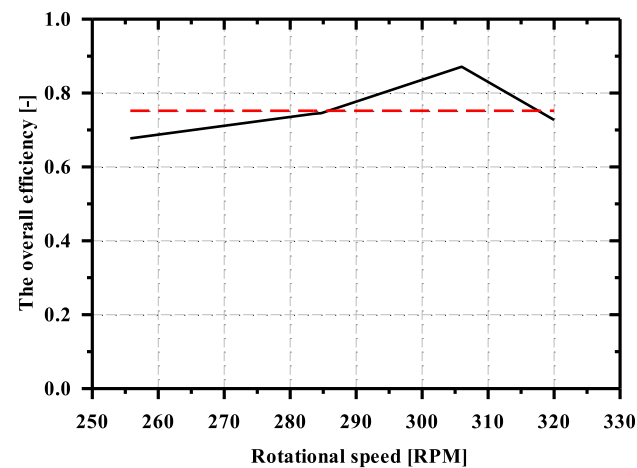


Fig. 9 The average overall efficiency through the system.

2.2. The turbine performance evaluation

The same spinning shaft connected a permanent magnet synchronous generator and the S-rotor blades. This alternative current (AC) generator was connected to a load board with lamps with direct-current (DC) power ranging from 10 to 500 W via a full-wave rectifier circuit, smoothing capacitors, voltage, and current measurements devices, as shown in Fig. 4. So, these lamps were used as an electric bulb circuit to get different tip speed ratios by controlling the rotor’s speed by adding an electric load gradually. The accuracy of the voltage and current measurements devices is ± 1 %.

The following equation expresses the relation between mechanical power extracted from the turbine and wind velocity passing through a turbine rotor plane [23]:

$$P_m = \frac{1}{2} \rho \pi R^2 V^3 C_{P_m} \tag{1}$$

where

P_m is the mechanical power that extracts from the turbine by the wind

, ρ is the air density in $\text{kg} \cdot \text{m}^{-3}$, R is the rotor radius, and C_{P_m} is the mechanical power coefficient. Also, the tip speed ratio is the ratio between the rotor velocity and the wind velocity and is expressed using the following equation:

$$\lambda = \frac{\omega R}{V} \tag{2}$$

The C_{P_m} value was given by [24] as follows:

$$C_{P_m} = 0.22 \left(\frac{116}{\lambda_i} - 0.4\beta - 5.0 \right) e^{-\frac{12.5}{\lambda_i}} \tag{3}$$

where,

$$\lambda_i = \left(\frac{1}{\lambda + 0.08\beta} - \frac{0.035}{\beta^3 + 1} \right)^{-1} \tag{4}$$

From the above equations, C_{P_m} is the function of the tip speed ratio, λ , and the pitch angle, β . The small wind pitch strategy in the field, especially the urban areas, was that if the wind velocity was less than the rated velocity of a wind turbine, as shown in this work, the pitch blade angle was kept constant at 0° to capture the maximum wind energy [25 26]. Therefore, the calculation is performed with the assumption that the optimal pitch angle of being $\beta = 0^\circ$. The S-rotor blade should be $\beta = 0^\circ$. Also, Fig. 5 showed that a pitch angle of 0° is the best-designed angle to capture the maximum power.

However, in this study, the power from the experimental work was measured based on the electrical load voltage and current after the rectifier, as shown in Fig. 4. The tip speed ratio is inversely proportional to the rotational speed for the constant wind velocity.

Fig. 6 showed the inverse relationship between the load current and the rotor speed in which, at low rotor speed, the load current increased. Also, the rotational speed was measured by a digital laser tachometer (omega, HHT13) with accuracy ± 0.01 of reading and a range of 5–200,000 rpm.

The electrical measurements were recorded when the system reached a steady-state condition. Hence, from the measured data, the electrical power coefficient (C_{P_e}) of the wind turbine was calculated. Fig. 7 showed the experimental output voltage and current of the PMSG. For Fig. 7 (a), the maximum



Fig. 10 The installation of the weather station on the Obour campus.

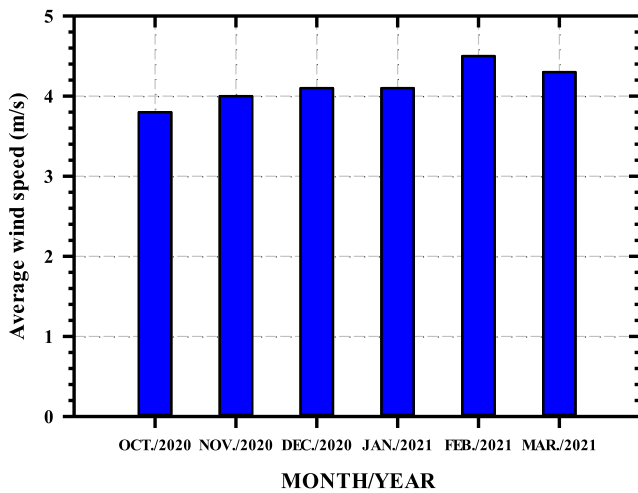


Fig. 11 Monthly statistics of average wind velocity.

obtained power at a wind velocity of 4 m/s was 89 W at (27.5 V and 3.24A). For Fig. 7 (b), the maximum obtained power at a wind velocity of 5 m/s was 163.9 W at (22 V and 7.45A). Also, for Fig. 7 (c), the maximum obtained power at wind velocity 6 m/s was 306 W at (34 V and 9A).

The electric system’s overall efficiency, defined as a ratio between the electrical power after the rectifier to the mechanical power before the electric generator, was used to compare the measured electrical power to the mechanically estimated ones. Figs. 8 and 9 studied the effect of the permanent magnet synchronous generator (type FD3.0–1000) and the rectifier circuit used in the current paper on the measurements. These figures showed that the electric system’s overall efficiency was about 75 % and was used to calculate all measured power coefficients.

The permanent magnet synchronous generator (PMSG) is the effective part of the calculating the electric system’s overall efficiency (η_0). This η_0 is consists of two efficiencies, the first is the synchronous generator efficiency (η_G), and the other is full-wave uncontrolled rectifier efficiency (η_R), whose value equals 0.9. And by using the following equation, the η_G can be calculated as follow:

$$\eta_G = \frac{\eta_0}{\eta_R} = \frac{0.75}{0.9} = 0.833 \quad (5)$$

The current open grid fans have a blockage ratio of 4 percent. As a result, the power coefficient measured in this work was corrected relating to these open grid fans. The blockage correction calculation was discussed in Eltayesh et al. [29]. Also, the estimations of uncertainty for the measured C_p in the experimental tests were carried out by Moffat’s formula [30]. The largest C_p uncertainty for the three input velocities investigated in this work is 1.28 %.

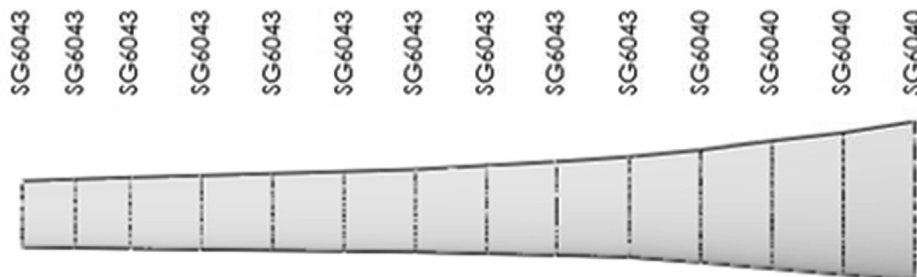


Fig. 12 Blade Model in QBlade Software.

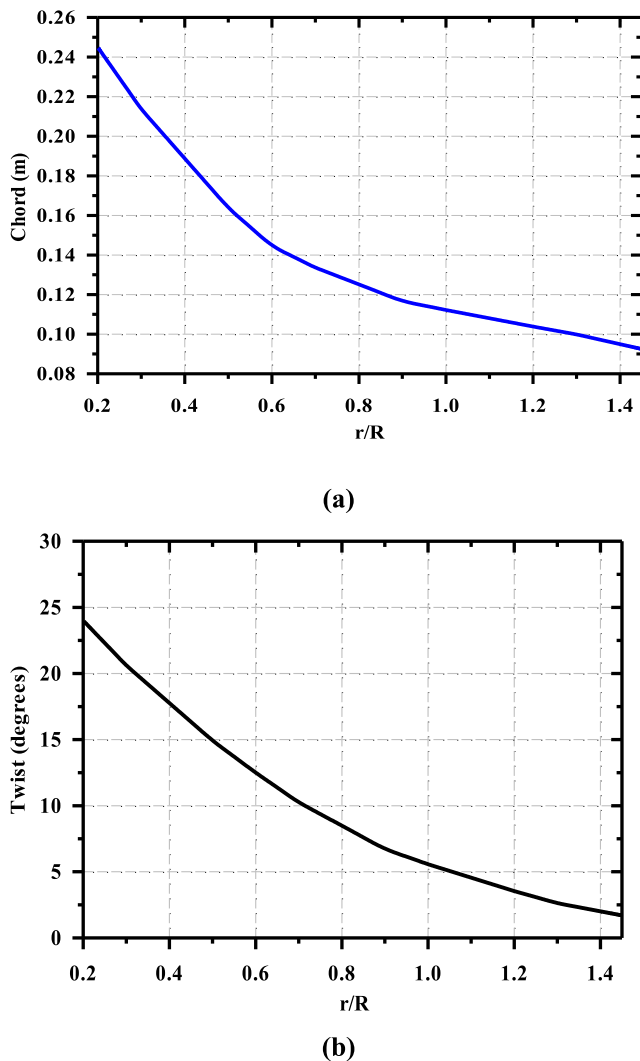


Fig. 13 Chord and twist distribution along the blade.

The commercial wind turbine with the specification shown in Table 1 has a rated wind velocity of 8 m/s. However, the residential areas haven't this velocity. Therefore, the (Davis vantage pro 2) weather station was used to measure the wind velocity in the Obour campus at Benha university, as shown in Fig. 10.

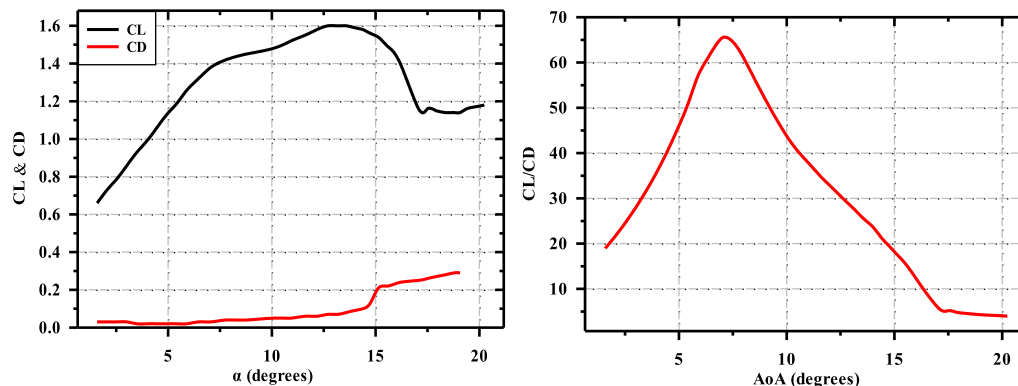


Fig. 14 Aerodynamic characteristics of the SG-rotor blade.

Based on the data collected from the weather station From October 2020 to March 2021, are shown in Fig. 11, the average wind velocity (\bar{V}) is about 4 m/s, so the new rotor is designed based on this predominant velocity by using an SG airfoil.

Egypt is one of the countries on the Red Sea and the Mediterranean with enough windy places. These locations, such as Ras Ghareb, where the average wind speed reached up to 12 m/s at 24.5 height and 15.5 m/s at 100 height above the ground in June [31]. Also, the wind speed data for Ras El-Hekma, Farafra, Nuweiba, and Aswan has been investigated using data measured at 50 m above sea level. The average wind speeds were 7, 6, 7, and 6, respectively [32]. Furthermore, the mean wind speed was measured for Abu Darag, Zafarana, G. EI-Zayt, and Hurgada with 4 stations, and the values were 9, 9.1, 10.4, and 6.9, respectively [33]. So, from the velocities of the wind in some locations in Egypt, the new rotor will also have the capability to work in these locations.

2.3. SG-rotor model

The aerodynamic design of the SG-rotor was performed by using the Q Blade software (V0.963) [34]. The Q Blade is open-source software for designing wind turbine blades and aerodynamical performance [35]. Lift (L) and Drag (D) forces are the two main components applied to any surface where the flow passes over it. Low wind velocities are generally defined for small wind turbine applications by airflows with Re less than 500,000 [6]. Low-angle-of-attack airfoils are used in low-velocity, small horizontal-axis wind turbines, resulting in a high lift coefficient (C_l) and low drag coefficient (C_d) [36].

SG6040 and SG6043 were selected from the NASA airfoil database for testing by using the Q Blade program, which was based on the x-foil tool, at a Re of 100,000 and an angle of attack of 7° . Power output primarily relied on L and D [37], so the lift coefficient should be maximized to improve wind turbine aerodynamic performance, and the drag coefficient should be minimized [38]. The 3D SG-rotor, as shown in Fig. 12, was created by using the selected airfoils that were distributed referring to [6] with an effective chord (c) as shown in Fig. 13 (a) and twist as shown in Fig. 13 (b) at each section along the blade.

The aerodynamic characteristics of the selected airfoils, such as lift coefficient (C_l), drag coefficient (C_d), and lift to

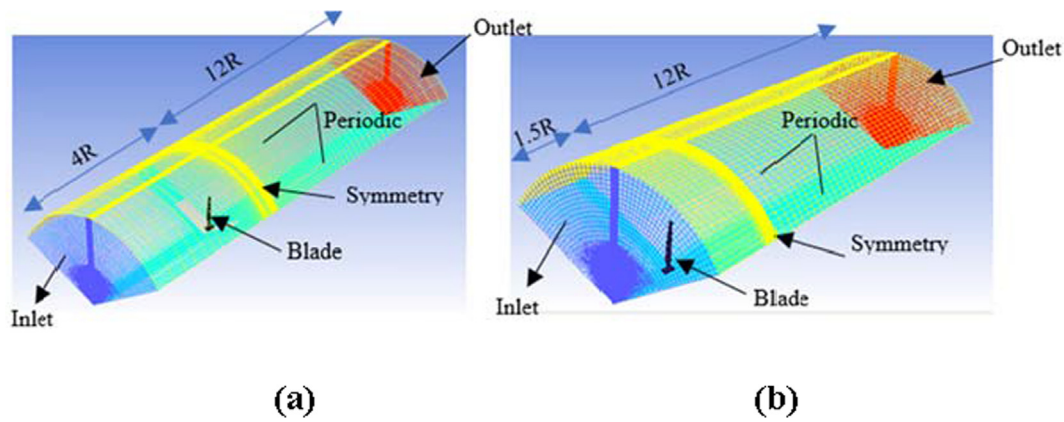


Fig. 15 The computational domain of the HAWT blade rotor.

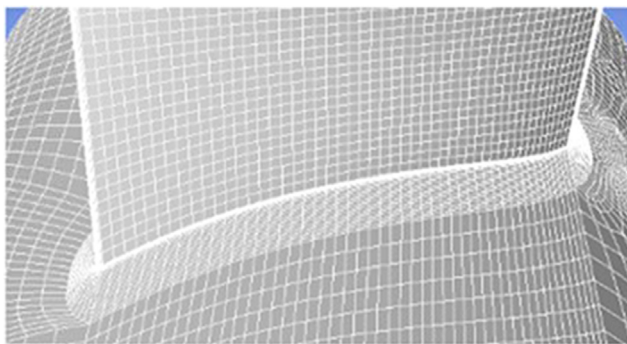


Fig. 16 The detail of the blade surface mesh.

drag coefficient was studied with different angles of attack from 1° to 20° , as shown in Fig. 14.

Fig. 14 depicted the SG-rotor had a high C_l of 1.6 at α of 13° as shown by the lift curve. The lift-to-drag ratio curve also showed that the SG-rotor's maximum lift-to-drag ratio value is 65.5 at α of 7° and that stall behavior was seen at angles rang-

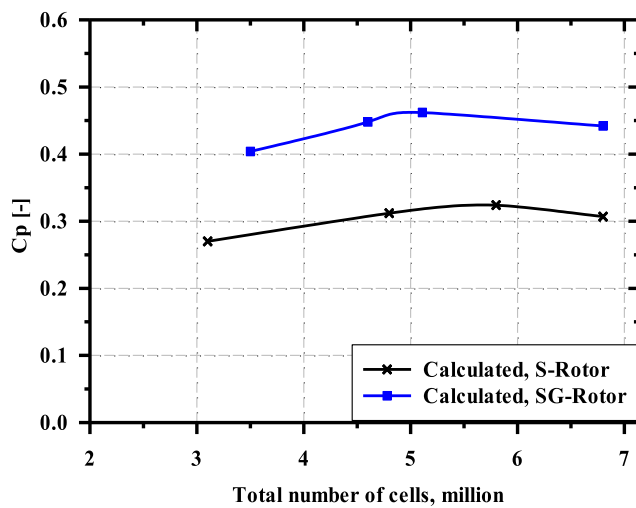


Fig. 17 Calculated power coefficient at a different grid resolution.

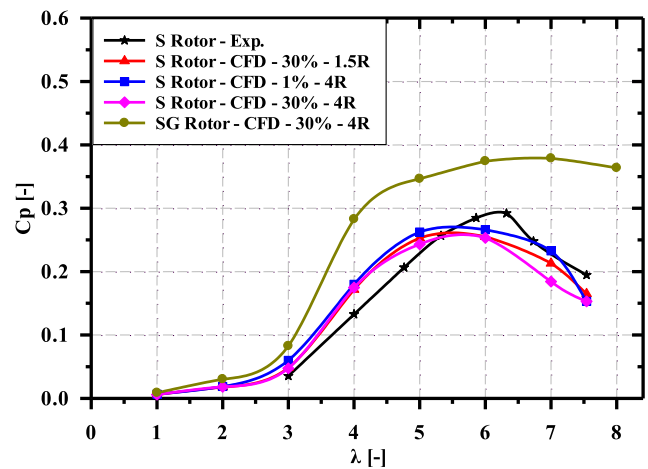


Fig. 18 The power coefficient vs the tip velocity ratio at 4 m/s.

ing from 8° to 16° . Due to its high lift-to-drag ratio, it might be deduced that the mixed airfoil was suited for low wind velocity applications.

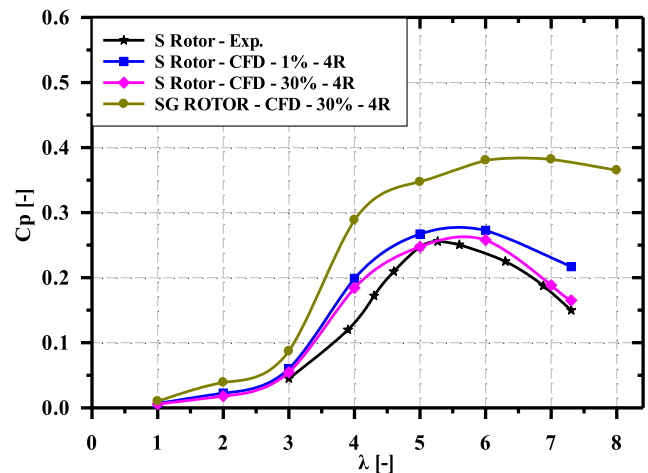


Fig. 19 The power coefficient vs the tip velocity ratio at 5 m/s.

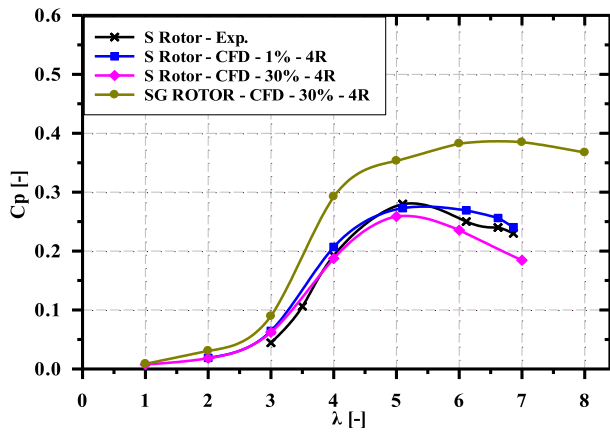


Fig. 20 The power coefficient vs the tip velocity ratio at 6 m/s.

3. Numerical simulation

For more observation of the flow behavior around wind turbine blades, numerical calculations were performed using the commercial CFD package Ansys Fluent version 18.1 [39] to study the aerodynamic performances of both HAWT rotors: S-rotor and SG-rotor. The 3D incompressible and steady flow is governed by the momentum and continuity conservation equations, as well as turbulence closure to obtain the flow characteristics. The SST k-omega turbulent model was used to solve the Reynolds-averaged Navier–Stokes (RANS) equations as introduced by [40 41]. The rotating wind turbine was modeled using the Moving Reference Frame (MRF) strategy. Eltayesh et al. [29] provide more information about MRF.

HAWT flow predictions have been reliably predicted using this method by numerous researchers Abdelwaly et al. [42].

3.1. Computational domain

The 3D computational domain and grid topology of the two-rotor geometry (S-rotor & SG-rotor) were generated using the gambit program, as illustrated in Fig. 15 (a). In the current work, the turbine blade and the hub were only simulated. The rest of the wind turbine, including the nacelle and tower, was not modeled. The inlet boundary condition based on the previous works [41,43,44] was set at 4 radius length from the center of the rotor, the outlet domain was set at 8 radius length, and in the radial directions, the domain was set at 2 radius length. However, to make the CFD model work under similar circumstances to the experimental condition, in the upstream, the domain was set 1.5 radius length of the turbine, as shown in Fig. 15 (b).

3.2. Grid generation

The grid generation was produced by using multi-blocks around the longitude of the blade. The rotor domain is divided into 102 blocks. The blocks adjacent to the turbine blade were generated using an O-grid structure [29,42,45] to fulfill the requirements for a fine grid and the dense mesh near the solid walls required to resolve the flow within the boundary layer over the blade, as shown in Fig. 16. The domain’s hybrid mesh topology was constructed. Close to the blade, a structured mesh with quadrilateral elements was applied to the block. Except for the blocks in the hub area, which used an

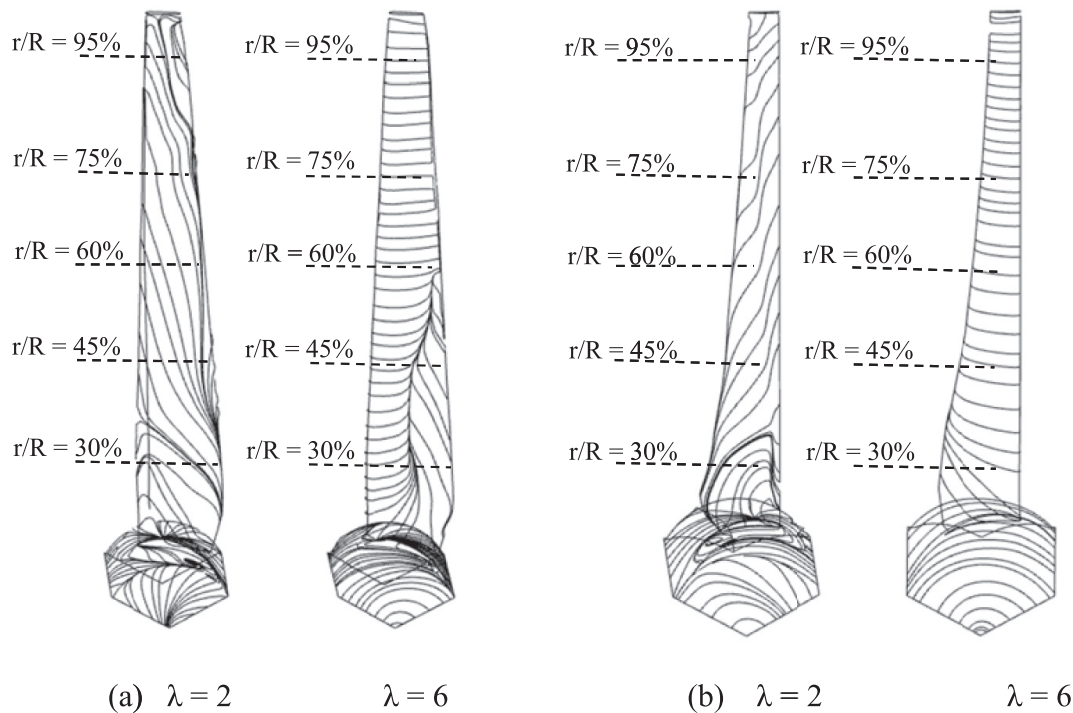


Fig. 21 The distribution of limiting streamlines on the suction surface of the blade at wind velocity of 4 m/s, λ of 2 and 6 for (a) S-rotor (b) SG-rotor.

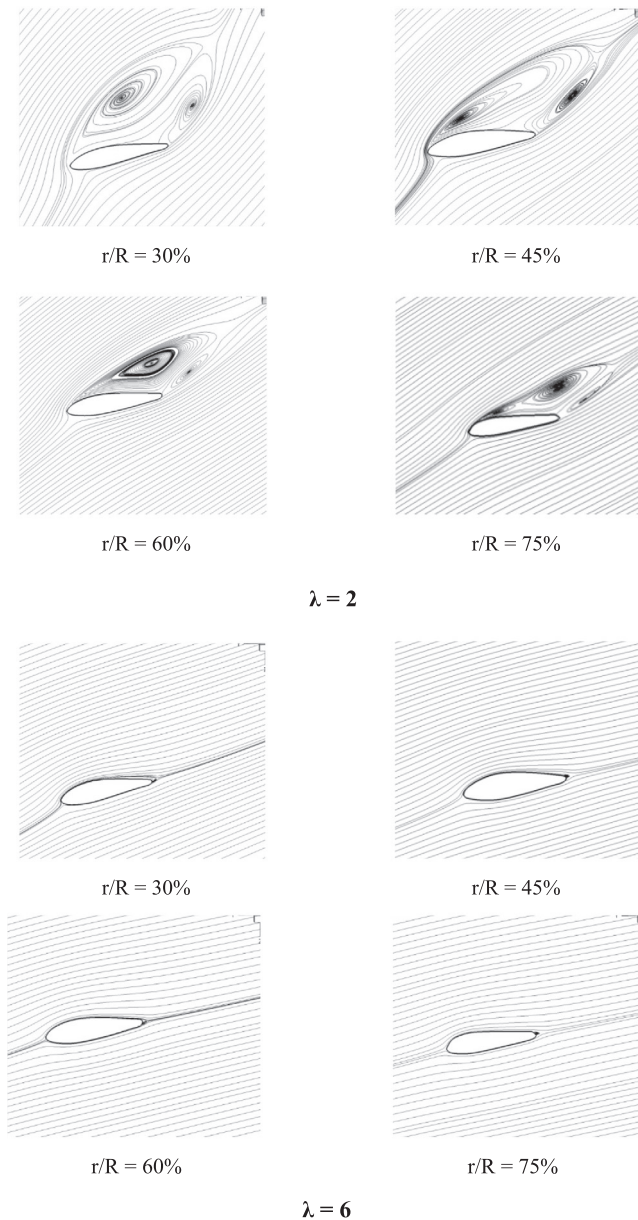


Fig. 22 The S-rotor's streamlines of relative velocity with λ of 2 and 6 and an inflow velocity of 4 m/s at various radial positions along the span.

unstructured mesh, the mesh for the blocks representing the inlet and outlet regions was structured.

The recommended near-wall distance for the grid spacing was constructed based on the recommendation introduced by Moshfeghi et al. [46]. A grid independence study was carried out to find suitable grid sizes required for the calculations. The grid study was performed at an inlet velocity of 4 m/s and a tip speed ratio of 5. Four different grid resolutions were used for S-rotor, with a total number of cells of 3.1, 4.8, 5.8, and 6.8 million. While 3.5, 4.6, 5.1, and 6.8 million cells were used SG-rotor as shown in Fig. 17. The figure demonstrated that by increasing the total number of grids above 5.8 million, the change in C_p was about 0.0118 for S-rotor. While an increasing number of cells above 5.1 million, the increase in

C_p is about 0.013 for SG-rotor. Consequently, from the grid dependency results, The S-rotor was meshed by 5.8 million cells, and the SG-rotor was meshed by 5.1 million cells which are pretty good as far as accuracy and economy of solution are concerned. Also, the $y^+ < 4$ for both rotors.

The incoming flow velocity was measured from the open grid fans experimentally, and then it was used to simulate the flow for the S-rotor and SG-rotor in CFD. In the present study, the uniform inlet velocity of 4, 5, and, 6 m/s is applied at the inlet boundary. The turbulent intensity had a significant impact on the performance of the SSHAWT [47], but it was hard to measure experimentally due to the unavailability of measuring devices. So it was estimated as introduced by [21]. Therefore, in this study, the test rig is made to simulate the wind pattern such as in the external aerodynamics flow and actual boundary layer, so the turbulent intensity was considered 30 %, and the comparison of the effect of the level of turbulent intensity was performed by using the CFD between 1 % and 30 %.

4. Results and discussion

Figs. 18-20 show the power coefficient of the S-rotor and SG-rotor at 4, 5, and 6 m/s, respectively. The measured power coefficient of the S rotor is also represented in Figs. 18- 20. To ensure the validity of the numerical methods, the numerical results for the S-rotor are compared with the experimental measurements at all wind velocities. The deviation between the experimental and numerical results is measured using the coefficient of correlation (R^2) method that was used by Abdelsalam et al. [22] for SSHAWT, which was computed from MainDonald and Braun [48] by:

$$R^2 = 1 - \frac{\sum (\phi_{exp.} - \phi_{num.})^2}{\sum (\phi_{exp.} + \bar{\phi}_{num.})^2} \quad (6)$$

where ϕ is the measured data, indicates here the power coefficient and $\bar{\phi}_{num.} = \frac{\sum_{i=1}^n \phi_{exp.}}{n}$, where n is the number of measured data.

For S-rotor, the value of (R^2) is 0.935, 0.95, and 0.923 for 4, 5, and 6 m/s, respectively. In general, a reasonable agreement of power coefficient was obtained between numerical calculations and experimental measurements, based to Abdelsalam et al. [22]. It can be observed that the SG-rotor has a superior power coefficient over the S-rotor for all inlet velocities. For 4 m/s, the maximum power coefficient ($C_{p_{max}}$) of the SG-rotor is 0.378 at λ of 7, while for S-rotor it is 0.253 at λ of 6, with an increase in the turbine performance of 62.2 %. While for 5 m/s, $C_{p_{max}}$ of the SG-rotor is 0.381 at λ of 7, while for S-rotor it is 0.258 at λ of 6, with an increase in the turbine performance of 61.9 %. While for 6 m/s, $C_{p_{max}}$ of the SG-rotor is 0.385 at λ of 7, while for S-rotor it is 0.2588 at λ of 5, with an increase in the turbine performance of 61.5 %.

Also, the effect of changing the turbulent intensity on the power coefficient is studied numerically, as shown in Figs. 18-20. The study is performed for the S-rotor in which the inlet boundary is set 4R from the rotor with the turbulence intensity levels of 1 % and 30 %. The figures showed that the use of turbulence intensity level of 30 % caused a reduction in wind turbine performance by 10.4 %, 14.65 %, and 11.4 %

compared to the turbulence intensity level of 1 % in winds of 4, 5, and 6 m/s, respectively.

Also, the effect of changing the distance between the inlet boundary and the rotor on the power coefficient is studied numerically to simulate the same condition of the experimental tests, as shown in Fig. 18. The study is performed for the S-rotor that was used in the experimental measurements at a wind velocity of 4 m/s. The coefficient of correlation (R^2) is calculated to find out the deviation in the numerical results when the distance between the inlet boundary and the rotor changes from 4R to 1.5 R on the power coefficient. The value of (R^2) is 0.984 and this means that the change of the inlet boundary condition has a neglected impact on the value of the power extracted.

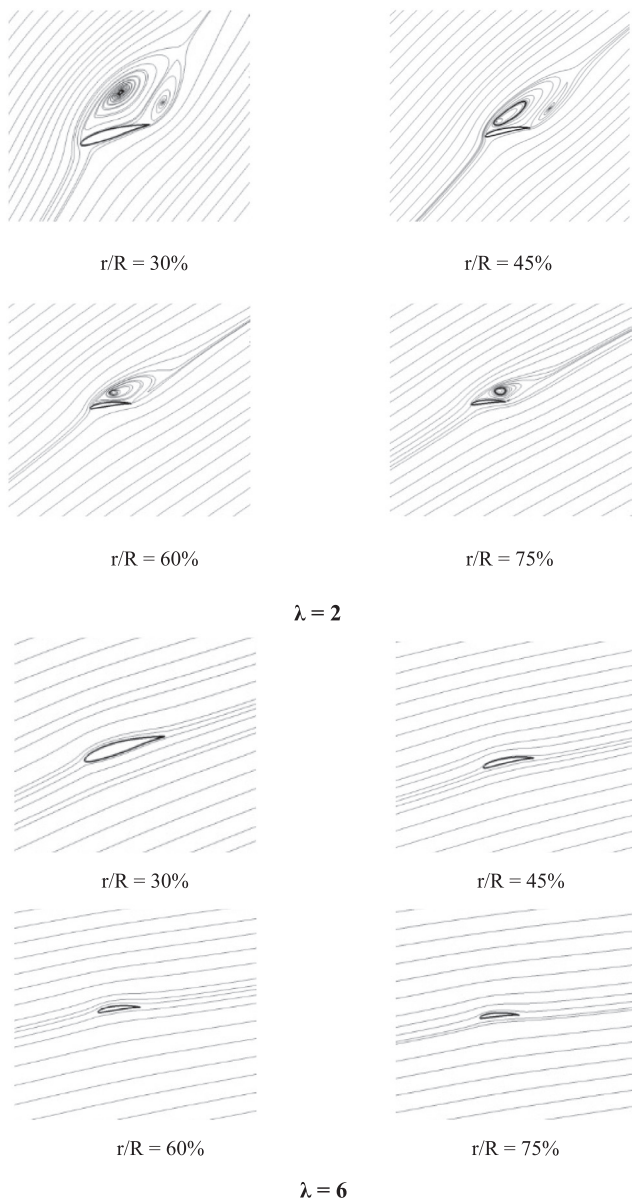


Fig. 23 The SG-rotor's streamlines of relative velocity with λ of 2 and 6 and an inflow velocity of 4 m/s at various radial positions along the span.

Wind turbine performance is affected by flow separation on the blade suction surface. Therefore, understanding the flow behavior would help a commercial wind turbine manufacturer. Fig. 21 shows the distribution of limiting streamlines on the suction surface of the blade when S and SG-rotors are at wind velocity of 4 m/s and different tip speed ratios. Fig. 21-a illustrates that at a low tip speed ratio of 2, the separation of the flow strongly occurs at the root close to the hub till nearly 75 % of the span of the S-rotor. Also, the radial flow is created and then moves along the entire blade surface. This shape may be occurred due to the increasing angles of attack at λ of 2. While with a high tip velocity ratio of 6, the separation occurs till r/R equal 60 %, but the stable flow occurs through the rest of the blade. However, by looking at Fig. 21-b and comparison with Fig. 21-a, it shows that the distribution of limiting streamlines for SG-rotor is more stable and smoother than for S-rotor along the entire suction surface blade.

Also, at various radii and tip-speed ratios, the corresponding flow streamline patterns around the blades are shown for the S-rotor and SG-rotor in Figs. 22 and 23, respectively.

Obviously, along the blade span at high tip speed ratios, the flow streamline patterns are attached to the blade profile in all cases. However, at lower tip velocity ratios and especially near the hub, the flow separation phenomena can be noticed based on Eltayesh et al. [44]. This phenomenon manifests more strongly for the S-rotor than the SG-rotor (which is the design case), even in high tip velocity ratios that occur near the trailing edges for all sections. This is possible because, in the new design (SG-rotor), the twist angle is designed to achieve a smooth connection to the hub.

Also, by looking at the reasons for the increase in the power coefficient, it is noted that the volume of the S-rotor is 0.0051 m^3 , but the SG-rotor is 0.0021 m^3 . So, the volume reduction by 58.8 %. As a result, the generated torque will increase, as discussed by Abdelsalam et al. [22].

5. Conclusions

In this study, a commercial SSHAWT with a rated power of 1 kW was tested in the laboratory at lower wind velocities of 4, 5, and 6 m/s. The experimental technique is based on the measurements of the output electrical power with the turbine tip speed ratio. The maximum measured power at these wind velocities was 306 W corresponding to a power coefficient of 0.28. The commercial SSHAWT showed significantly reduced performance of this rotor at lower wind velocities than the rated velocity. The CFD numerical simulations were also performed, verified the same conclusion, and showed good agreement with the experimental studies.

A new design for the rotor is proposed, which is referred to here as SG-rotor and is examined using CFD numerical simulations, and the results showed significant improvement for the new design rotor performance compared to the commercial rotor. The results showed that at wind velocities of 4, 5, and 6 m/s, the maximum power coefficients of the SG-rotor were 0.378, 0.381, and 0.385 at a designed tip speed ratio of 7, respectively. While the power coefficient of the commercial S-rotor was 0.253, 0.258, and 0.2588 at tip speed ratios ranging from 5 to 6.

A comprehensive investigation of flow streamlines behavior is conducted in detail for the two rotors. The results concluded

that the flow separation phenomena manifested most strongly for the S-rotor than the SG-rotor, particularly at lower tip velocity ratios and near the hub. Furthermore, the SG-rotor had a lower manufacturing cost, with the expectation of a lower cut-in velocity resulting from the SG-volume rotor, which was reduced by 58.8 % compared to the S-rotor. For the future works, it is recommended to investigate the performance of the new SG-rotor experimentally, determine its cut-in velocity and study the stresses that affect the turbine. Also, more tests will be performed outdoor.

Declaration of Competing Interest

The authors declare that they have no known competing financial interests or personal relationships that could have appeared to influence the work reported in this paper.

Acknowledgement

The authors extend their appreciation to the Scientific Research fund at Benha University for funding this work through the Research Support Program.

References

- [1] T.G. Wang, L. Wang, W. Zhong, B.F. Xu, L. Chen, Large-scale wind turbine blade design and aerodynamic analysis, *Chinese Sci. Bull.* 57 (5) (2012) 466–472, <https://doi.org/10.1007/s11434-011-4856-6>.
- [2] V.J. Kurian, S.P. Narayanan, C. Ganapathy, Towers for offshore wind turbines, *AIP Conf. Proc.*, vol. 1225, no. June 2010, pp. 475–487, 2010, doi: 10.1063/1.3464894.
- [3] N.G. Mortensen, U.S. Said, J. Badger, *Wind Atlas for Egypt*, 2006.
- [4] A. Tummala, R.K. Velamati, D.K. Sinha, V. Indrajaya, V.H. Krishna, A review on small scale wind turbines, *Renew. Sustain. Energy Rev.* 56 (2016) 1351–1371.
- [5] L.C. Pagnini, M. Burlando, M.P. Repetto, Experimental power curve of small-size wind turbines in turbulent urban environment, *Appl. Energy* 154 (2015) 112–121, <https://doi.org/10.1016/j.apenergy.2015.04.117>.
- [6] P. Giguère, M.S. Selig, New airfoils for small horizontal axis wind turbines, *J. Sol. Energy Eng. Trans. ASME* 120 (2) (1998) 108–114, <https://doi.org/10.1115/1.2888052>.
- [7] R. Kumar Gupta, V. Warudkar, R. Purohit, S. Singh Rajpurohit, Modeling and Aerodynamic Analysis of Small Scale, Mixed Airfoil Horizontal Axis Wind Turbine Blade, *Mater. Today Proc.* 4 (4) (2017) 5370–5384, <https://doi.org/10.1016/j.matpr.2017.05.049>.
- [8] Y.Y.H. Aung, M.M. Soe, A.M. Thu, Effect of Attack angle on Aerodynamics Analysis of Different Wind Turbine Wings using Numerical Simulation, *Am. Sci. Res. J. Eng. Technol. Sci.* 26 (4) (2016) 319–329.
- [9] N. Karthikeyan, T. Suthakar, Computational studies on small wind turbine performance characteristics, *J. Phys.: Conf. Ser.* 759 (2016) 012087, <https://doi.org/10.1088/1742-6596/759/1/012087>.
- [10] R. Nath, S. Bhattacharjee, Computational intelligence for numerical analysis of wind energy conversion system, pp. 130–136, 2018.
- [11] M. Ould Moussa, Experimental and numerical performances analysis of a small three blades wind turbine, *Energy* 203 (2020), <https://doi.org/10.1016/j.energy.2020.117807>.
- [12] H.H. Mwanyika, Y.A. Jande, T. Kivevele, Design and Performance Analysis of Composite Airfoil Wind Turbine Blade, *Tanzania J. Sci.* 47 (5) (2021) 1701–1715, <https://doi.org/10.4314/tjs.v47i5.18>.
- [13] M.K. Chaudhary, S. Prakash, S. Kushawaha, L. Gupta, P. Humbre, A.N. Patil, Numerical and experimental analysis of a small horizontal axis wind turbine rotors, *AIP Conf. Proc.*, vol. 2311, no. December, 2020, doi: 10.1063/5.0034317.
- [14] M. Sessarego, D. Wood, Multi-dimensional optimization of small wind turbine blades, *Renewables* 2 (1) (2015), <https://doi.org/10.1186/s40807-015-0009-x>.
- [15] M. Hasan, A. El-Shahat, M. Rahman, Performance Investigation of Three Combined Airfoils Bladed Small Scale Horizontal Axis wind Turbine by BEM and CFD Analysis, *JPEE* 05 (05) (2017) 14–27.
- [16] M.S. Selig, B.D. McGranahan, Wind tunnel aerodynamic tests of six airfoils for use on small wind turbines, *J. Sol. Energy Eng. Trans. ASME* 126 (4) (2004) 986–1001, <https://doi.org/10.1115/1.1793208>.
- [17] D.S. Pamuji, M.A. Bramantya, Numerical Study on the Performance Of 2-Bladed and 3-Bladed Counter Rotating Wind Turbines, *J. Japan Soc. Appl. Electromagn. Mech.* 27 (1) (2019) 169–174, <https://doi.org/10.14243/jsaem.27.169>.
- [18] B. Li, J. Liu, J. Gao, Surface wind pressure tests on buildings with various non-uniformity morphological parameters, *J. Wind Eng. Ind. Aerodyn.* 137 (2015) 14–24, <https://doi.org/10.1016/j.jweia.2014.11.015>.
- [19] https://www.ouyad.com/WindTurbine_160.html.
- [20] S. El-Shahat, H. El-Batsh, A. Attia, G. Li, L. Fu, “Experimental and Numerical Investigations of Pressure Loss and 3-D Flow Separations in a Linear, Compressor Cascade” (2019), <https://doi.org/10.1115/IMECE2019-10686>.
- [21] C. Michael and W. Torsten, “Ercoftac Best Practice guidelines for Cfd.” p. 94, 2000.
- [22] A.M. Abdelsalam, W.A. El-Askary, M.A. Kotb, I.M. Sakr, Experimental study on small scale horizontal axis wind turbine of analytically-optimized blade with linearized chord twist angle profile, *Energy* 216 (2021) 119304, <https://doi.org/10.1016/j.energy.2020.119304>.
- [23] I. Munteanu, A. Bratcu, N. Cutululis, E. Ceanga, Optimal control of wind energy systems: towards a global approach, 2009.
- [24] T. Sun, Power Quality of Wind Connected Wind Turbines with DFIG and their Interaction with the Grid, vol. Doctor of. 2004
- [25] X. Gao, X. Wang, J. He, R. Weerasinghe, J. Wu, C.-H. Weng, Optimal control of pitch angle of large wind turbine based on speed differential, *E3S Web Conf.* 194 (2020) 03008, <https://doi.org/10.1051/e3sconf/202019403008>.
- [26] P.A.C. Rocha, J.W. Carneiro de Araujo, R.J.P. Lima, M.E. Vieira da Silva, D. Albiero, C.F. de Andrade, F.O.M. Carneiro, The effects of blade pitch angle on the performance of small-scale wind turbine in urban environments, *Energy* 148 (2018) 169–178, <https://doi.org/10.1016/j.energy.2018.01.096>.
- [27] O.E. Gouda, E.M. Saied, O.M. Salim, M.I. Awaad, Grid Side Converter Controller Optimized for DFIG Driven Wind Turbine Based on Type-2 Fuzzy Logic, vol. 7, no. 4, pp. 810–816, 2016
- [28] O. E. Gouda, O. M. Salim, and M. Awaad, “Type-2 Fuzzy Logic Application of a Grid Side Converter Control for DFIG Driven Wind Turbines,” no. December, 2015.
- [29] A. Eltayesh, M.B. Hanna, F. Castellani, A.S. Huzayyin, H.M. El-Batsh, M. Burlando, M. Becchetti, Effect of wind tunnel blockage on the performance of a horizontal axis wind turbine with different blade number, *Energies* 12 (10) (2019) 1988, <https://doi.org/10.3390/en12101988>.
- [30] R.J. Moffat, Describing the uncertainties in experimental results, *Exp. Therm. Fluid Sci.* 1 (1) (1988) 3–17, [https://doi.org/10.1016/0894-1777\(88\)90043-X](https://doi.org/10.1016/0894-1777(88)90043-X).

- [31] A.S. Ahmed, Electricity generation from the first wind farm situated at Ras Ghareb, Egypt, *Renew. Sustain. Energy Rev.* 16 (3) (2012) 1630–1635, <https://doi.org/10.1016/j.rser.2011.12.002>.
- [32] M.H. Alham, M.F. Gad, D.K. Ibrahim, Potential of wind energy and economic assessment in Egypt considering optimal hub height by equilibrium optimizer, *Ain Shams Eng. J.* no. xxxx (2022), <https://doi.org/10.1016/j.asej.2022.101816> 101816.
- [33] N. G. Mortensen and U. S. Said, “Wind atlas for the Gulf of Suez. Measurements and modelling 1991-1995,” vol. ISBN87-550, pp. 1–110, 2002.
- [34] D. Marten, “QBlade v0.9: Guidelines,” p. 37, 2015.
- [35] M. Alaskari, O. Abdullah, M.H. Majeed, Analysis of Wind Turbine Using QBlade Software, *IOP Conf. Ser.: Mater. Sci. Eng.* 518 (3) (2019) 032020, <https://doi.org/10.1088/1757-899X/518/3/032020>.
- [36] C. Thumthae, T. Chitsomboon, Optimal angle of attack for untwisted blade wind turbine, *Renew. Energy* 34 (5) (2009) 1279–1284, <https://doi.org/10.1016/j.renene.2008.09.017>.
- [37] S.A. Kale, M. Birajdar, S.N. Sapali, Numerical Analysis of New Airfoils for Small Wind Turbine Blade, *J. Altern. Energy Sources Technol.* 6 (1) (2016) 1–6.
- [38] T. Uchiyama, H. Yagami, Numerical Simulation of Low Reynolds Number Particle-Laden Gas Jet by Vortex Method, *J. Fluid Sci. Technol.* 4 (2) (2009) 335–347, <https://doi.org/10.1299/jfst.4.335>.
- [39] ANSYS® Academic Research Mechanical, Release 18.1 Help System, Coupled Field Analysis Guide, ANSYS, Inc.
- [40] P.I. Muiruri, O.S. Motsamai, Three dimensional CFD simulations of a wind turbine blade section; validation, *J. Eng. Sci. Technol. Rev.* 11 (1) (2018) 138–145, <https://doi.org/10.25103/jestr.111.16>.
- [41] M.H. Lee, Y.C. Shiah, C.J. Bai, Experiments and numerical simulations of the rotor-blade performance for a small-scale horizontal axis wind turbine, *J. Wind Eng. Ind. Aerodyn.* 149 (2016) 17–29, <https://doi.org/10.1016/j.jweia.2015.12.002>.
- [42] M. Abdelwaly, H. El-Batsh, M. Bassily Hanna, Numerical study for the flow field and power augmentation in a horizontal axis wind turbine, *Sustain. Energy Technol. Assessments*, vol. 31, no. December 2018, pp. 245–253, 2019, doi: 10.1016/j.seta.2018.12.028.
- [43] R.P.J.O.M.V. Rooij, E.A. Arens, Analysis of the experimental and computational flow characteristics with respect to the augmented lift phenomenon caused by blade rotation, *J. Phys.: Conf. Ser.* 75 (2007) 012021, <https://doi.org/10.1088/1742-6596/75/1/012021>.
- [44] A. Eltayesh, F. Castellani, M. Burlando, M. Bassily Hanna, A.S. Huzayyin, H.M. El-Batsh, M. Becchetti, Experimental and numerical investigation of the effect of blade number on the aerodynamic performance of a small-scale horizontal axis wind turbine, *Alexandria Eng. J.* 60 (4) (2021) 3931–3944, <https://doi.org/10.1016/j.aej.2021.02.048>.
- [45] C. Method, “Aerodynamic Improvements of Wind-Turbine Airfoil Geometries,” 2011.
- [46] M. Moshfeghi, Y.J. Song, Y.H. Xie, Effects of near-wall grid spacing on SST-K- ω model using NREL Phase VI horizontal axis wind turbine, *J. Wind Eng. Ind. Aerodyn.* 107–108 (2012) 94–105, <https://doi.org/10.1016/j.jweia.2012.03.032>.
- [47] M.S. Siddiqui, A. Rasheed, T. Kvamsdal, M. Tabib, Effect of turbulence intensity on the performance of an offshore vertical axis wind turbine, *Energy Procedia* 80 (1876) (2015) 312–320, <https://doi.org/10.1016/j.egypro.2015.11.435>.
- [48] J. Maindonald, J. Braun, Data analysis and graphics using R: an example-based approach, vol. 10. Cambridge University Press, 2006.